Journal of Molecular Modeling (2022) 28: 59
https://doi.org/10.1007/s00894-022-05048-4

ORIGINAL PAPER

Polythiophene as a sensor model for chlorofluorocarbon, fluorine, and oxygen gas using DFT calculations

Md. Mehade Hasan[1,2] · Shahida Akter Bithe[1] · Budrun Neher[2] · Farid Ahmed[2]

Received: 20 December 2021 / Accepted: 4 February 2022 / Published online: 14 February 2022

Abstract

Adsorption of CCl_3F, CCl_2F_2, $CClF_3$, F_2, and O_2 has been investigated systematically on the polythiophene (PT) moieties using density functional theory (DFT) calculations at the B3LYP/6-31G (d) level. Here, geometry optimizations have been performed on some polythiophene (5PT and 7PT) complexes. Likewise, adsorption energies, dipole moments, HOMO–LUMO orbital analysis, density of states (DOSs), global indices, and UV–vis spectra are calculated using the DFT method. Energies of interaction and HOMO–LUMO gap show that polythiophene has the highest sensitivity toward O_2 for B3LYP functional. According to our findings, CFCs, F_2, and O_2 molecules can be physically adsorbed on the moieties of polythiophene.

Keywords Polythiophene · DFT · Chlorofluorocarbon · Fluorine · Oxygen · Gas sensor

Introduction

Gas sensors are a kind of sensing device or component of a safety system used to detect hazardous gases in the surrounding environment. By including a guidance system, this kind of apparatus may be used to monitor the presence of gas and modify a process on an automated basis. In the past several years, a slew of research articles with encouraging results have been published, all of which have highlighted the different features of gas sensors [1–3]. When it comes to gas sensor design for material selection, the primary goal of molecular modeling is to provide a theoretical underpinning. The use of experimental data is required when modeling first principles concerning physical features that are hypothesized to be present. Traditionally, quantum mechanics and the availability of an adequate force field (a mathematical depiction of the energy of a molecule as a function of geometry) are required for this. Besides, it may contain equations of Hamilton's motion equations (Newtonian classical molecular dynamics). Additionally, the first-principles analysis may be employed to identify the interactions among analytes that are bound with vapor and different (discrete or coupled) organic moieties embedded in polymer sensors without any experimental validation. This information may be used to conduct research aimed at enhancing the raw material selection process. We are planning to go that route in this present investigation [4].

Neutral polymers are often regarded as materials capable of serving as semiconducting or insulating materials. Their ability to be converted into thoroughly conductive materials is a promising development with conductivity comparable to metals confiding based on n-doping or p-doping, yet those are light and resilient compared to metals when it comes to physical characteristics [5]. Conducting polymer-based sensors is increasingly extensively utilized due to their electrical characteristics, including a fast reaction time and excellent stability [6]. On the other hand, polymer conductors may be manipulated in sensor moiety manufacturing [7]. According to some research, the electrical and optical characteristics of conductive polymers, contrasted with non-conductive polymers, are very appealing [8]. Due to these promising properties, polymer-based sensors are now the focus of the majority of research. Polymers are widely used in the manufacture of thin-film transistors [9], light-emitting polymer diodes [10], corrosion resistance [11], electromagnetic shielding [12], sensor technology [13], molecular electronics [14], supercapacitors [15], and etc.

✉ Md. Mehade Hasan
mehade@just.edu.bd; mehade.36@gmail.com

[1] Department of Physics, Jashore University of Science and Technology, Jashore 7408, Bangladesh

[2] Department of Physics, Jahangirnagar University, Dhaka 1342, Bangladesh

Polythiophene, an appealing adsorbent for various researchers toward gas sensing, is utilized as a filter for poisonous substances in numerous shapes of composition and derivatives. Owing to the bewitching electrical, chemical, and physical characteristics, recent advancements in the development of fundamental conductive polymers such as polyaniline (PANI), polythiophene (PT), polypyrrole (PPy), and their derivatives have been made [16–20]. Figure 1 shows the ChemDraw structures of 5PT and 7PT respectively.

Chlorofluorocarbons (CFCs) are a family of chemicals consisting of volatile methane and ethane derivatives and brominated and chlorinated elements. Consequently, the standard formulae of CFCs can be indicated as CCl_nF_{4-n} and $C_2Cl_nF_{6-n}$ with a non-zero estimation of n. The growing usage of CFCs will result in the ozone layer of the atmosphere being depleted, which was anticipated in 1974 [21]. As a consequence of their chemical stability, CFCs may constantly disperse and be carried from the lower climate (i.e., the troposphere) to the upper environment (i.e., the stratosphere). Chlorine atoms are released as a result of CFC photolysis. Following that, these chlorine atoms undergo a number of further reactions that lead to the breakdown of ozone in the atmosphere. Overall, these chain reactions have been identified as having critical roles in stratospheric ozone depletion, which are now being studied further [22].

Several decades after the discovery of CFCs in the mid-1930s, the practice of using CFCs extensively for household and industrial applications arose as a result of their novel properties such as low flammability, the low thermal conductivity of the gas phase, low toxicity, low corrosiveness during use, good chemical inertness, and reasonable cost, among others [23]. The systematic name of CFC-11, CFC-12, and CFC-13 are trichlorofluoromethane, dichlorodifluoromethane, and chlorotrifluoromethane with chemical formulae CCl_3F, CCl_2F_2, and $CClF_3$ respectively. Diverse applications for these CFCs include usage as refrigerants, solvents, propellants, and foam blowing agents [24].

When it comes to refrigerants, CFC-11 is favored over CFC-115, but then when it comes to propellants, CFC-11/12 is chosen over CFC-114. Regardless of the fact that preferences between comparable goods differ, the majority of these gases are capable of meeting the wide range of needs from businesses and consumers. The carbon tetrachloride (CCl_4), which has the characteristic of being the most influential hepatotoxic of all the main CFC compounds, has been utilized as fire extinguishers, cleaning fluid, and fumigant since the early 1900s. In recent years, the usage of CFCs has grown to include a wider range of industrial operations, as well as the production of CFCs itself (CFC-11 and CFC-12) [25, 26]. Besides being used as a refrigerant, CFC-12 was also extensively used as an aerosol propellant, which is less well-known [27, 28]. In addition, the CFC-13 is extensively used as a refrigerant since it is non-flammable, non-corrosive, and includes a combination of halomethanes [29]. Usually, CFCs enter the human body mostly via direct inhalation of CFC-containing air or through skin contact with CFCs. Inhaling large quantities of CFCs may have a detrimental effect on the lungs, central nervous system, heart, liver, and kidneys. Excessive exposure to CFCs may result in fatal illness and even death [30]. The table below shows the chemical formula and common name of some CFCs to get a clear idea about some other CFCs.

Systematic name	Common name	Chemical formula
Trichlorofluoromethane	CFC-11	CCl_3F
Dichlorodifluoromethane	CFC-12	CCl_2F_2

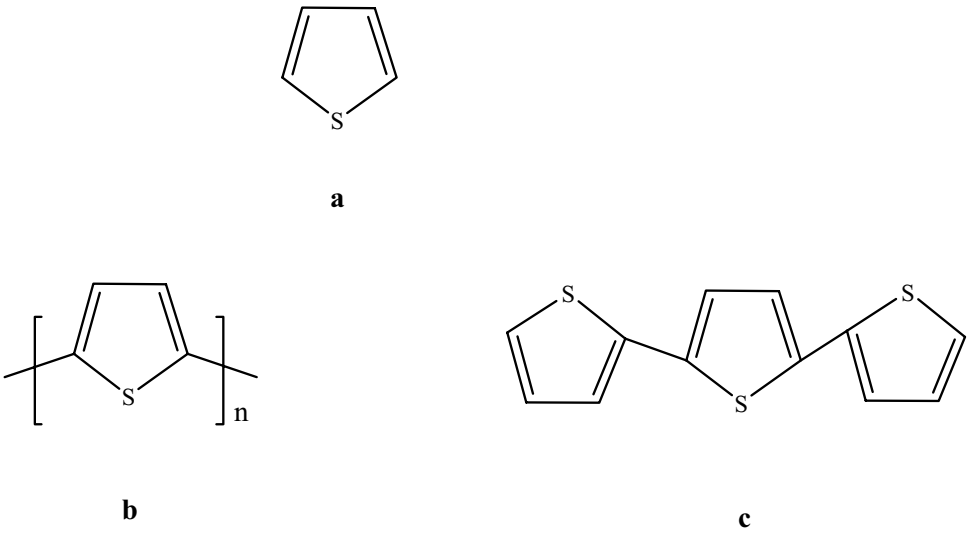

Fig. 1 ChemDraw structures of polythiophene. a Monomer. b Polymer. c 3PT (where 3 is the number of associated rings of PT)

Systematic name	Common name	Chemical formula
Chlorotrifluoromethane	CFC-13	$CClF_3$
Tetrachloro-1,2-difluoroethane	CFC-112	CCl_2FCCl_2F
1,1,2-Trichloro-1,2,2-trifluoro-ethane	CFC-113	$Cl_2FC\text{-}CClF_2$
1,2-Dichloro-1,1,2,2-tetrafluor-oethane	CFC-114	$ClF_2C\text{-}CClF_2$
1-Chloro-1,1,2,2,2-pentafluor-oethane	CFC-115	$ClF_2C\text{-}CF_3$

Furthermore, fluorine is a trace element that exists in a non-metallic diatomic gas, which is a non-metallic compound. It is a highly flammable, toxic light yellow gas. Explosions occur when fluorine reacts directly with alkali metals. The fluorine molecule is chemically the most reactive element and it is the most powerful known oxidizing agent except for a few lanthanide and actinide ions and the XeF molecule. It is also a highly electronegative atom—but it is a poor hydrogen bond acceptor in organic molecules due to its low charge capacity, which limits the negative character that it can achieve [31]. A large amount of fluorite, the main source of fluorine, is used extensively in fabricating steel products. Numerous medications have been discovered to contain fluorine, and fluorine's interaction with the bulk of standard materials is highly corrosive. Fluorine combines with water under normal circumstances. When it is exposed to explosive materials over an extended length of time, it becomes unstable and fluorine has the ability to ignite the vast majority of them due to its oxidizing properties. Fluorine containers may explode if exposed to fire or heat for a prolonged period. If breathed or absorbed via the skin, fluorine may cause very toxic and deadly effects. Chemical burns can occur as a result of low concentrations of fluorine exposer. Osteosclerosis and calcification of ligaments may occur as a consequence of repeated absorption. Fluorine, acting as an oxidant, promotes excitability [32].

Additionally, surface corrosion and heterogeneous catalysts are two examples of how the interaction of oxygen on metal and metal-like surfaces is significant from a number of viewpoints [33]. Because of this, there is much interest in the literature to develop a novel surface for use as an O_2 adsorbent/sensor [30, 34].

We are going to investigate polythiophene (PT) moiety interactions with CFCs, F_2, and O_2 molecules in this existing research. To gain a deeper comprehending of the connection between chemical structure and characteristics, we have provided first-principles analysis on PT moieties as a simple polythiophene model in both free and coupled modes with CFC-11, CFC-12, CFC-13, F_2, and O_2. To the best of our knowledge, no prior research has been conducted on the sensing activity of PT toward CFCs, F_2, or O_2.

Computational methods

The system geometries and characteristics were determined using DFT calculations on the 6-31G (d) basis set with the B3LYP functional and implemented in the Gaussian 09 software [35]. For the accuracy in analyzing various nanostructures, B3LYP is a trustworthy functional in the 6-31G (d) basis set [36]. A further reason for selecting the DFT technique was the fact that it is generally trusted and produces accurate findings [37].

Mulliken and NBO charge analysis, the density of states (DOS), lowest unoccupied molecular orbital (LUMO) energy, highest occupied molecular orbital (HOMO) energy, bandgap energy (E_g), recovery time (τ), sensitivity (σ) and global indices (like hardness, softness, chemical potential, electrophilicity), and UV–vis spectra are going to estimate at the above-stated level of theory. Materials Studio 7.0 has been used to adsorb CFCs, F_2, and O_2 gases on the PT moieties. GaussSum 2.2 [38] has been used to intrigue the density of states (DOS) and UV–vis spectra. Moreover, cohesive energy (E_{Coh}) and adsorption energy (E_{ads}) determine the investigated systems' reliable stability. The cohesive energy (E_{Coh}) of the nanostructures is calculated as [39]:

$$E_{Coh} = \left(E_{nPT} - xE_S - yE_C - zE_H\right)/m \tag{1}$$

where n (= 5, 7) is the number of associated rings of the PT structures (5PT and 7PT); E_{nPT} is the energy of the PT structures; E_S, E_C, and E_H represent the energy of isolated sulfur, carbon, and hydrogen atom respectively; x, y, and z are the numbers of sulfur, carbon, and hydrogen atoms respectively of the studied moieties and the total number of constituent atoms of the corresponding moieties is represented by m.

The adsorption energy (E_{ads}) and the change of enthalpy (ΔH) of CFCs, F_2, and O_2 on the isolated PT moiety can be defined by the following equations [40]:

$$E_{ads(nPT)} = E_{nPT-X} - \left(E_{nPT} + E_X\right) \tag{2}$$

$$\Delta H_{(nPT-X)} = H_{nPT-X} - \left(H_{nPT} + H_X\right) \tag{3}$$

$E_{ads\,(nPT-X)}/\Delta H_{(nPT-X)}$ are the adsorption energy/change of enthalpy for X species (CFCs, Cl_2, and O_2) on nPT moieties. E_{nPT-X}/H_{nPT-X} is the energy/enthalpy of nPT-X complexes, E_{nPT}/H_{nPT} are the energy/enthalpy of isolated nPT molecule, and E_X/H_X represents the energy of the X species. The interaction energy is negative, which means that the most stable structure has the lowest energy.

The chemical potential (μ) is computed in accordance with the provided formula [38]:

$$\mu = \frac{E_{\mathrm{HOMO}} + E_{\mathrm{LUMO}}}{2} \tag{4}$$

where E_{HOMO} stands for the energy associated with the highest occupied molecular orbital (HOMO), and E_{LUMO} indicates the energy of the lowest unoccupied molecular orbital (LUMO).

Furthermore, using the Koopmans theorem [41] hardness (η) can be calculated as:

$$\eta = \frac{E_{LUMO} - E_{HOMO}}{2} \tag{5}$$

Softness (S) [41] and electrophilicity (ω) [41] are characterized respectively as the following equations:

$$S = \frac{1}{2\eta} \tag{6}$$

$$\omega = \frac{\mu^2}{2\eta} \tag{7}$$

To help visualize the direction of electron flow, the fractional change in transmitted electron number (ΔN) has been summarized as [42]:

$$\Delta N = \frac{\mu_B - \mu_A}{\eta_B + \eta_A} \tag{8}$$

Here, the global hardness and chemical potential of species A (gas molecules) and B (moieties for 5PT and 7PT) are denoted by η and μ, respectively. On the other hand, the function of reactivity descriptors, namely the total change of stabilization energy ($\Delta E_{SE(AB)}$), change of the energy of species A ($\Delta E_{A(B)}$), and change of the energy of species B ($\Delta E_{B(A)}$), was also produced to know the stability of the studied structures with the help of the following equations [43–45]:

$$\Delta E_{A(B)} = \Delta N(-\mu_A + \frac{1}{2}\eta_A \Delta N) \tag{9}$$

$$\Delta E_{B(A)} = \Delta N(-\mu_B + \frac{1}{2}\eta_B \Delta N) \tag{10}$$

$$\Delta E_{SE(AB)} = \Delta E_{A(B)} + \Delta E_{B(A)} = \frac{-(\mu_B - \mu_A)^2}{2(\eta_B + \eta_A)} \tag{11}$$

In order to determine the adsorption energy of a complex system (E_{ads}), it is essential to first understand the adsorption process of the complex system in which it occurs. The recovery time (τ) is the amount of time needed to liberate gas molecules after adsorption, whereas it is coupled to E_{ads} as follows [46]:

$$\tau = \nu_0^{-1} \exp(\frac{-E_{ads}}{KT}) \tag{12}$$

where T, ν, and k ($\sim 2 \times 10^{-3}$kcal/mol) represent the temperature, the attempt frequency, and the Boltzmann constant consequently. According to Eq. (12), there is an exponential relationship between τ and E_{ads}. And the more negative values of adsorption energies are responsible for higher recovery time. If the recovery time is considerable, this means that the adsorbent must be exposed to the adsorbate molecules for a much more extended period of time that is a common reason why a longer time period is incompatible with gas detection applications. Table 2 summarizes the recovery times in the range of several nanoseconds (ns) to picoseconds (ps) under vacuum ultraviolet light conditions ($\nu \sim 10^{12}$s^{-1}) for the investigated complexes at room temperature, acknowledging 5PT and 7PT moieties' rapid recovery from CFCs, F_2, and O_2 gas molecules which is quite significant.

We investigated the sensitivity of 5PT and 7PT polythiophene moieties toward CFCs, F_2, and O_2 gas molecules by the connection between electronic conductivity (σ) and bandgap (E_g) as [47, 48]:

$$\sigma \; \alpha \; \exp(\frac{-E_g}{2KT}) \tag{13}$$

where k denotes the Boltzmann constant and T denotes the temperature, respectively. Equation (13) illustrates the exponential connection between E_g and σ, showing that a lower E_g value corresponds to improved electrical conductivity. In Fig. 2, the model structure of 5PT and 7PT has been shown to understand the structure clearly.

Results and discussion

Optimized geometry with adsorption energy, enthalpy, and frequency

By observing the adsorption energy of a complex system, we can comprehend how well an adsorbent is interacting with adsorbate in a complex system. The better adsorbent structure is shown by a more negative adsorption energy value [49]. The interactions of CFCs, F_2, and O_2 gas molecules with nPT have been studied and allowed to be completely optimized using the methods mentioned above. Following optimization of 5PT and 7PT, we chose a more consistent one for further study. The objective of Fig. 1 is to illustrate how nPT atoms are numbered during their interaction with the species mentioned above. Typical optimized configurations are shown in the top and side views in Fig. 2 for 5PT-CFC-11, 5PT-CFC-12, 5PT-CFC-13, 5PT-F_2, and 5PT-O_2. Table 1 represents the interaction energies calculated using the B3LYP functional. Since adsorption energy with a higher negative value correlates to adsorption energy

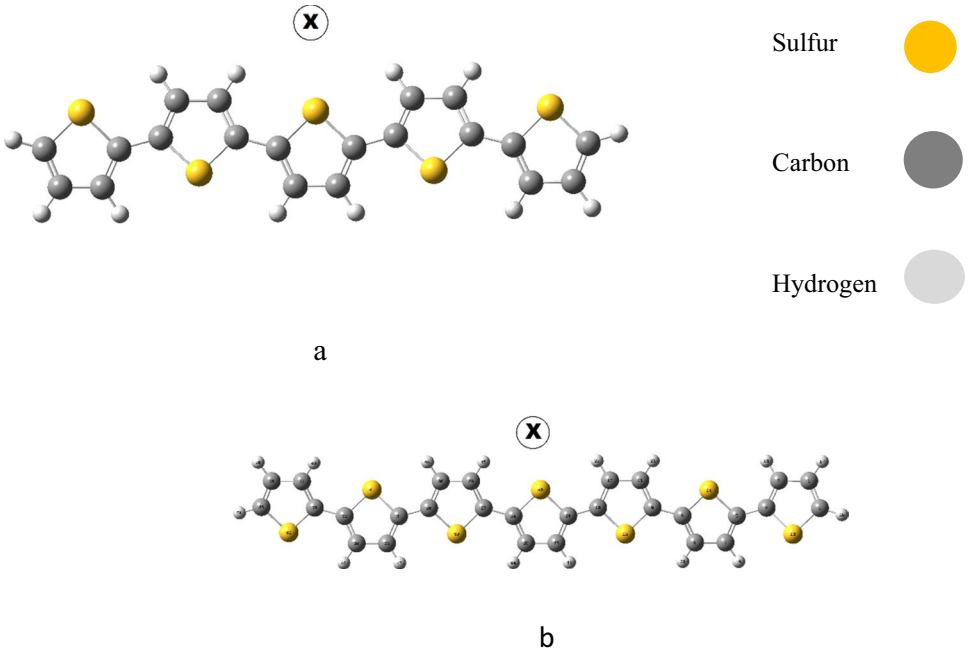

Fig. 2 The structure of a 5PT and b 7PT (X here is known as the dummy atom as apart from analyte)

Table 1 Mulliken, natural bond orbital (NBO), HOMO energy (E_{HOMO}), LUMO energy (E_{LUMO}), the energy of Fermi level (E_{FL}), energy gap (E_g), and dipole moment (μ_D) and adsorption energy (E_{ad}) of nPT-X ($n=5$ and 7), and X = CFC-11, CFC-12, CFC-13, F_2, and O_2 complexes

System/properties	$Q_{Mulliken\ (e)}$	NBO	$E_{HOMO\ (eV)}$	$E_{FL\ (eV)}$	$E_{LUMO\ (eV)}$	$E_{g\ (eV)}$	μ_D(Debye)	E_{ad} (kJ mol^{-1})
CFC-11	−0.195	−0.315	−8.829	−5.291	−1.752	3.534	0.175	-
CFC-12	−0.352	−0.648	−9.036	−5.086	−1.136	3.950	0.075	-
CFC-13	−0.654	−1.050	−9.473	−4.831	−0.188	4.643	0.232	-
F_2	−0.342	−0.001	−4.784	−4.042	−3.30	0.742	0.689	-
O_2	−0.001	−0.001	−6.807	−5.843	−4.878	0.965	0.00	-
5PT	−0.342	−0.456	−4.902	−3.467	−2.033	2.869	0.832	-
5PT-CFC-11	−0.342	−0.459	−4.941	−3.505	−2.069	2.872	0.386	−2.179
5PT-CFC-12	−0.350	−0.645	−4.878	−3.444	−2.009	2.869	0.865	−6.220
5PT-CFC-13	−0.681	−1.048	−4.898	−3.450	−2.002	2.896	0.826	−11.966
5PT-F_2	−0.342	−0.461	−4.911	4.116	−3.320	1.592	0.834	−5.285
5PT-O_2	−0.341	−0.475	−5.118	−4.161	−3.204	1.914	1.861	−22.722
7PT	−0.342	−0.456	−4.774	−3.502	−2.230	2.544	0.625	-
7PT-CFC-11	−0.342	−0.457	−4.811	−3.529	−2.246	2.565	0.994	−2.032
7PT-CFC-12	−0.350	−0.646	−4.760	−3.484	−2.207	2.553	0.314	−6.057
7PT-CFC-13	−0.677	−1.052	−4.810	−3.502	−2.195	2.615	0.721	−7.484
7PT-F_2	−0.342	−0.461	−4.784	−4.057	−3.330	1.454	0.689	−5.212
7PT-O_2	−0.341	−0.475	−4.940	−4.075	−3.211	1.730	1.953	−22.785

with a higher strength, the energy for 5PT shows the order of 5PT-CFC-11 < 5PT-F_2 < 5PT-CFC-12 < 5PT-CFC-13 < 5PT-O_2. In the case of 7PT, the complexes show the same order as the complexes of 5PT. In both the 5PT and 7PT, we get higher adsorption energy for oxygen, while in both cases, we get lower adsorption energy for CFC-11. To comprehend the nature of adsorption, we scrutinized the change in enthalpy (ΔH) and found negative values for most of the studied complexes except for CFC-11 which indicates their exothermic nature of the interaction.

The CFC-11, CFC-12, CFC-13, F_2, and O_2 molecules adsorbed on the moiety of 5PT with adsorption energies (E_{ads}) of −2.179, −6.220, −11.966, −5.285, and −22.722 kJ mol^{-1} and the moiety of 7PT with adsorption energies (E_{ads}) of −2.032, −6.057, −7.484, −5.212, and −22.785 kJ mol^{-1} respectively. Here we see the highest

adsorption energy is − 22.785 kJ mol^{-1} among all complexes, and it confirms that all the studied complexes represent weak physisorption type adsorption because we know when a complex shows adsorption energy less than 1 eV or 96 kJ mol^{-1}, it is considered physisorption, and greater than that value is called chemisorption [50]. Based on our result, it can be confirmed that the adsorption and desorption processes of all studied gas molecules occur quickly, which establishes the reversibility of 5PT and 7PT moieties.

Moreover, to obtain the local minima structure, it was necessary to conduct a frequency calculation on all adsorbed gases (gas molecules), adsorbent molecules (5PT and 7PT), and corresponding complexes. It was discovered that there is no imaginary frequency observable for the selected structures (shown in Fig. 3), revealing the actual minima structure.

Dipole moment and molecular electrostatics potential

The findings of Table 1 show the evaluated dipole moments (μ_D) for CFCs (CFC-11, CFC-12, and CFC-13), F_2, and O_2 on nPT moieties. The word "dipole moment" refers to the distinctive characteristics of a molecule that take geometry into consideration [51, 52]. More complex polarity usually correlates with more dipole moments. Our studies show that when the CFCs, F_2, and O_2 species were closed on the moieties of isolated 5PT and 7PT, the size and directions of μ_D were altered based on the property of interaction and the quantity of charge transfer which affects the polarity of the complex formed. Our investigation exhibited that the dipole moment increased for most systems (except 5PT-CFC-11, 5PT-CFC-13, 7PT-CFC-12) upon adsorption of CFCs, F_2,

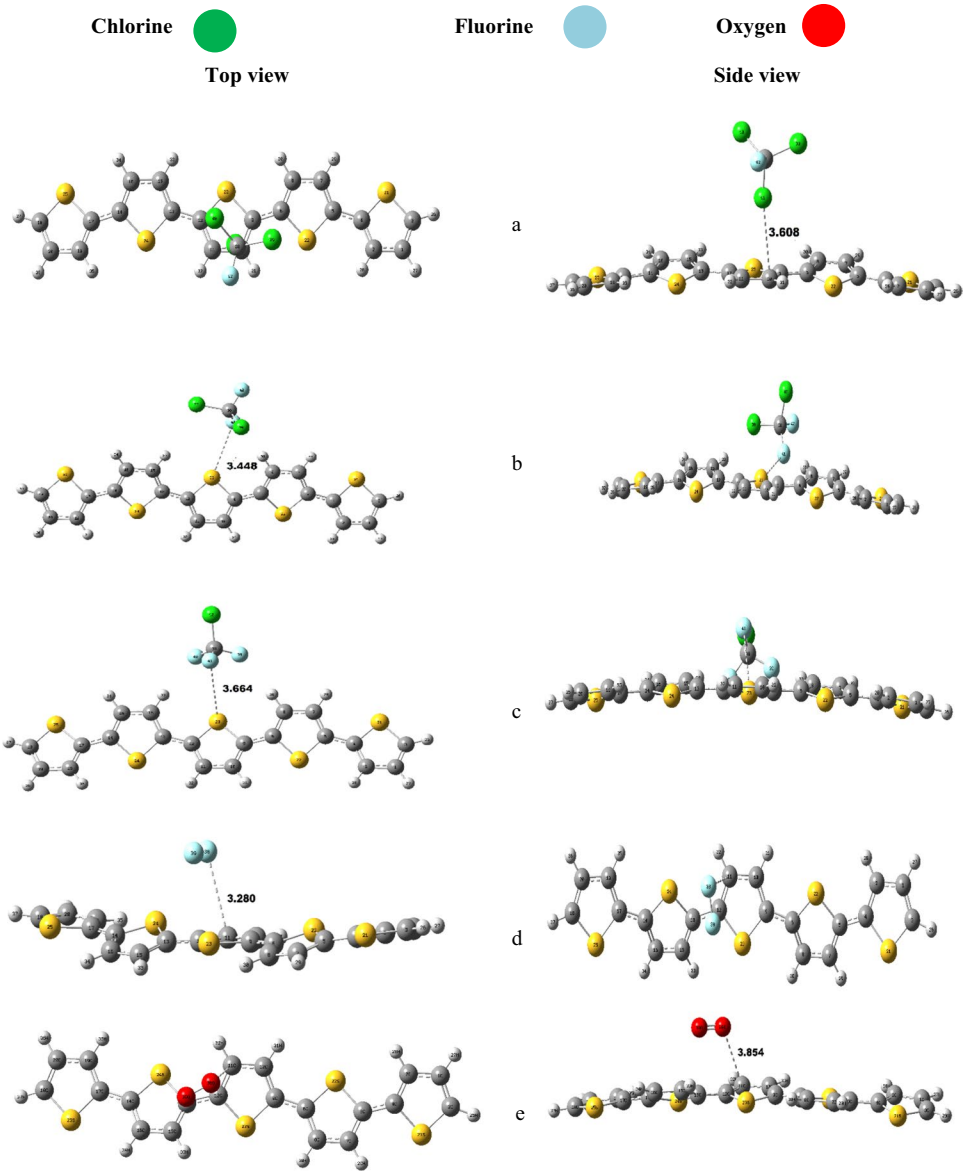

Fig. 3 The optimized constructions of a 5PT-CFC-11, b 5PT-CFC-12, c 5PT-CFC-13, d 5PT-F2, and e 5PT-O2 are shown in the top and side views, respectively

and O_2 molecules. The calculated values of μ_D for isolated 5PT and 7PT were 0.832 and 0.625 Debye, respectively, so the complex forms of nPT show more stability than those of the isolated conditions. To know the binding sites of a molecule (model monomer and polythiophene) deeply, the molecular electrostatic potential (MEP) has also been investigated as shown in Fig. 4. A most significant parameter of the electrostatic potential is that it is a real physical property which is also observable. Moreover, HOMO is not a reliable guide to find out the most reactive sites toward electrophiles [53–55]. Another one thing is that the MEP maps represent the electron density distribution over molecules in which the positive region (blue color) indicates the cationic environment while the negative region (red color) indicates the accumulation of electronic charges [56].

Orbital analysis

To better understand orbital hybridization and altered energy gaps, we performed an orbital analysis using the HOMO and LUMO distributions for isolated 5PT and complex forms (5PT-CFC-11, 5PT-CFC-12, 5PT-CFC-13, 5PT-F_2, and 5PT-O_2) of the species, which are illustrated in Fig. 5 below. Our analysis team observed that the values of calculated energies of HOMO and LUMO for isolated 5PT and 7PT are − 4.902 and − 4.774 eV and − 2.033 and − 2.230 eV, respectively. An increase is shown in the HOMO (LUMO) of 5PT on sensing CFC-11, F_2, and O_2 and decrease on CFC-12 and CFC-13 molecules with the values of 0.039 (0.036), 0.009 (1.287), 0.216 (1.171), 0.024 (0.024), and 0.004 (0.031) eV respectively. The investigated data confirms that the HOMO energies for 7PT increased for all complexes except 7PT-CFC-12 and further confirms that the energies of LUMO for 7PT decrease for 7PT-CFC-12 and 7PT-CFC-13 but increase for 7PT-CFC-11, 7PT-F_2, and 7PT-O_2 complexes. In the case of nPT-F_2 and nPT-O_2, the LUMO is primarily located on the F_2, O_2 ring, and interactive polythiophene ring, respectively. In the case of CFCs, the LUMO is found on polythiophene rings.

HOMO–LUMO energy gap (E_g) is not the one and only parameter for determining the electronic stability of resulting interactions rather than considering free space in the crystal lattice of the explosive instead of single molecular or crystal property, a strongly positive electrostatic potential associated with the central portion of the molecular surface, a high detonation heat release; but we have calculated this (E_g) parameter to observe their nature of sensitivity [53] [57]. The estimated E_g value for isolated 5PT and 7PT is 2.869 and 2.544 eV, respectively. As shown in Table 1, the bandgap of both the 5PT and 7PT increased for CFC-11 and CFC-13, and decreased for F_2 and O_2, while the CFC-12 showed no change after adsorption on 5PT.

As a result of our estimations, we have learned that CFC interactions with 5PT and 7PT are roughly comparable to the bandgaps of both solitary nPTs, with the exception of O_2 and F_2, which have a more significant impact. However, based on the kind of analyte, the bandgap of the resulting complex is different from that of the lone nPT. We may assert (but not always) that when the difference between the bandgaps of the analyte and the adsorbent is less, the change in their complex bandgap is greater (more hybridizing), as is evident with F_2 and O_2 on both moieties. A lower bandgap means higher electrical conductivity, and a higher bandgap, in contrast, means lower electrical conductivity [58, 59], so it may be inferred that, among the investigated complexes, 7PT-F_2 has the greatest conductivity and 5PT-CFC-13 has the lowest conductivity. As interacting with different analytes, the nPT Fermi level value changes. This simple example demonstrates that complex systems have a higher concentration of electrons or holes than solitary nPT systems.

Density of states (DOS) analysis

The DOS spectra of both solitary and complex forms of nPT are plotted and shown in Fig. 6 to provide a thorough knowledge of the interaction phenomenon/electronic characteristics of nPT-X structures and assess bandgap fluctuation (DOS of 7PT shown in Supplemental materials). Following the DOS plots and bandgap, we discovered that when

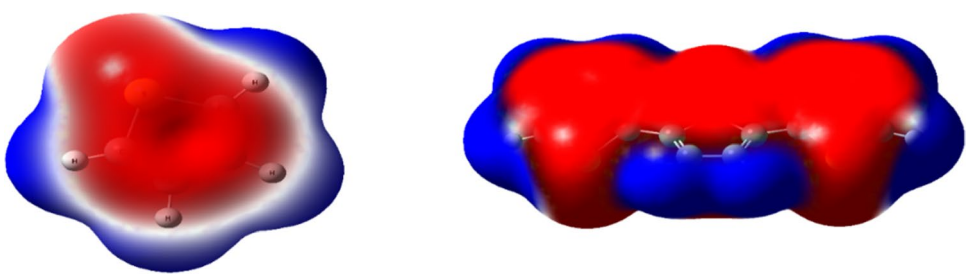

a b

Fig. 4 MEP of a monomer and b a model polythiophene of 3PT (combined structure of 3 monomers) on 0.001 au molecular surface

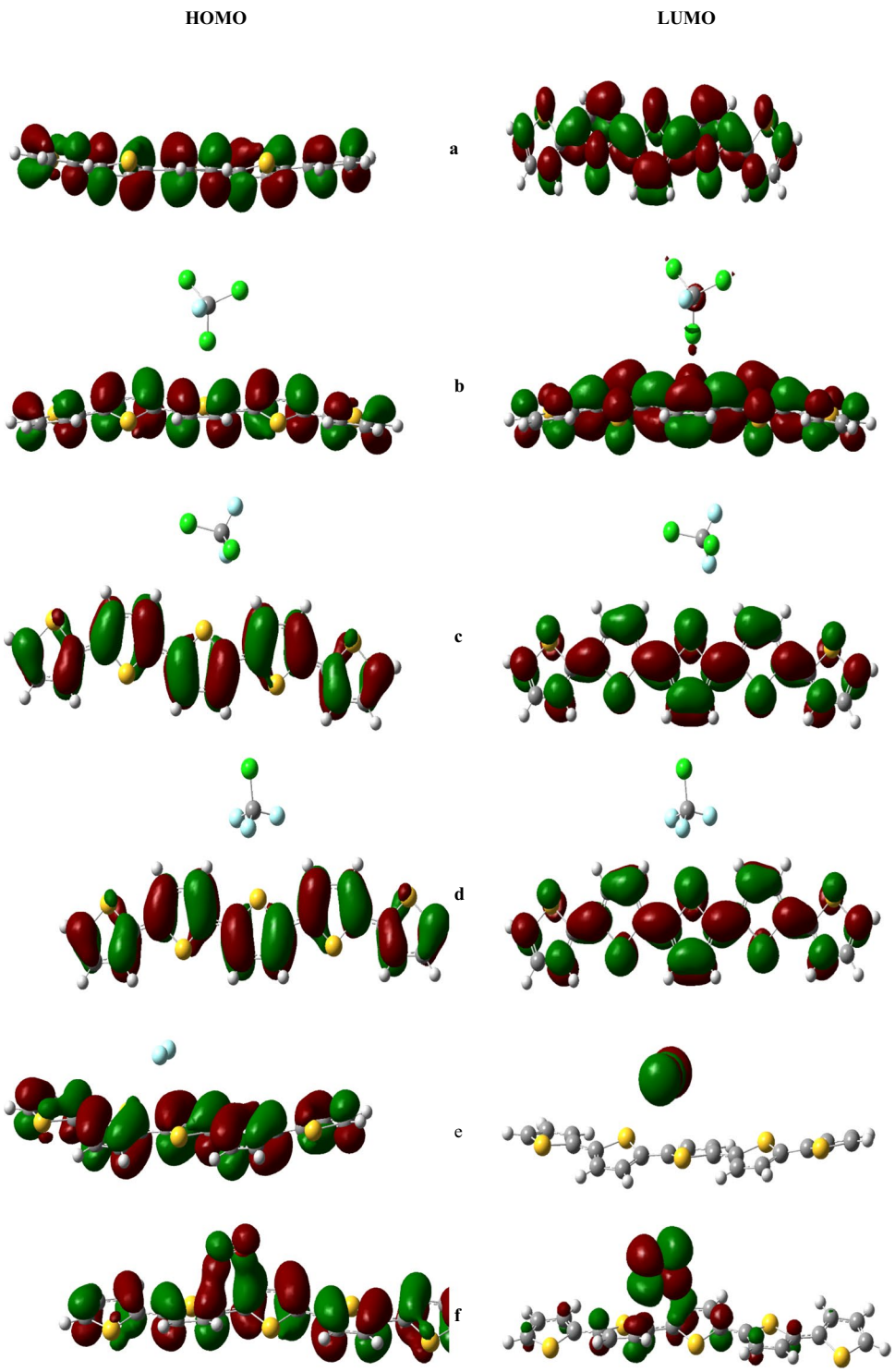

Fig. 5 The top and side views of the HOMO and LUMO density distributions for the following systems: a 5PT, b 5PT-CFC-11, c 5PT-CFC-12, d 5PT-CFC-13, e 5PT-F2, and f 5PT-O2, respectively

gas molecules interact with nPT, there is a minimal indication of hybridization for CFC-12. A further finding of our research is that the bandgaps of solitary and complex forms of nPT are virtually identical to one another. As a result, the electrical structure of nPT is not substantially changed. The physical contact between species and nPT is shown by this observable behavior.

Chemical potential and global indices

The chemical potential (μ), global hardness (η), global softness (S), and electrophilicity (ω) of nPT have been calculated by using Eqs. (4), (5), (6), and (7), respectively, as shown in Table 2. If the chemical potential of the structure decreases, the reactivity of the structure decreases, thereby

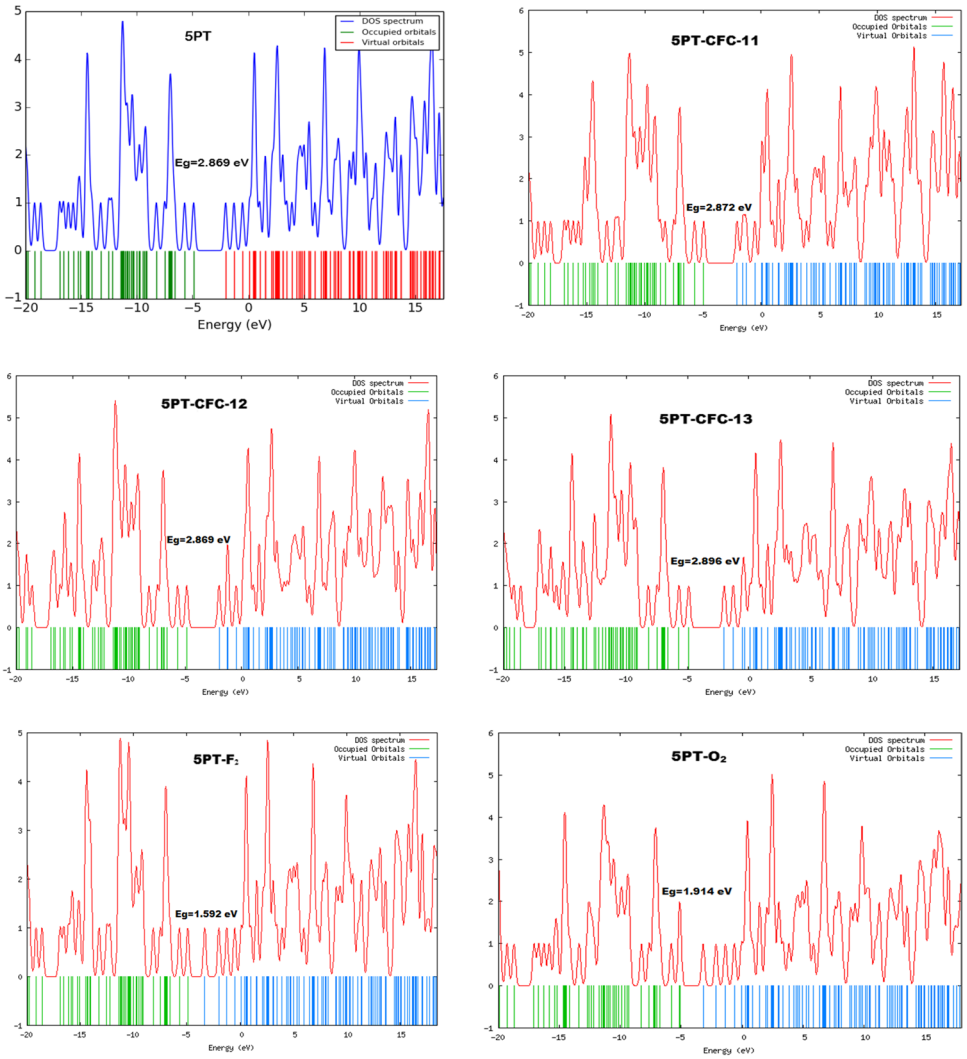

Fig. 6 DOS spectra of all systems (of 5PT) using B3LYP functionals

Table 2 Chemical potential (μ), electronegativity (χ), hardness (η), softness (S), and electrophilicity (ω), thermodynamic parameters of each system upon adsorption enthalpy change (ΔH, kJ mol^{-1}), recovery time (τ) of nPT-X ($n=5$ and 7), and X=CFC-11, CFC-12, CFC-13, F_2, and O_2 at the B3LYP/6-31G (d) level of theory

System/property	μ (eV)	X	η (eV)	S (eV^{-1})	ω (eV)	ΔH(kJ mol^{-1})	τ(ns/ps)
CFC-11	−5.291	5.291	3.539	0.141	3.955	-	-
CFC-12	−5.086	5.086	3.950	0.127	3.274	-	-
CFC-13	−4.831	4.831	4.643	0.108	2.513	-	-
F_2	−4.042	4.042	0.742	0.674	11.009	-	-
O_2	−5.843	5.843	0.965	0.518	17.696	-	-
5PT	−3.467	3.467	1.435	0.348	4.190	-	-
5PT-CFC-11	−3.505	3.505	1.436	0.348	4.278	0.673	79.8 ps
5PT-CFC-12	−3.444	3.444	1.434	0.349	4.134	−0.225	4.03 ps
5PT-CFC-13	−3.450	3.450	1.448	0.345	4.109	−1.545	0.404 ps
5PT-F_2	−4.116	4.116	0.796	0.628	10.642	−0.330	8.324 ps
5PT-O_2	−4.161	4.161	0.957	0.522	9.044	−4.605	9.062 ns
7PT	−3.502	3.502	1.272	0.393	4.821	-	-
7PT-CFC-11	−3.529	3.529	1.282	0.390	4.855	0.707	0.101 ps
7PT-CFC-12	−3.484	3.484	1.277	0.392	4.753	−0.195	8.63 ns
7PT-CFC-13	−3.502	3.502	1.307	0.382	4.691	−0.605	0.946 ns
7PT-F_2	−4.057	4.057	0.727	0.688	11.317	−0.014	8.085 ps
7PT-O_2	−4.075	4.075	0.865	0.578	9.603	−4.606	9.294 ns

the stability increases [60, 61]. In this manner, 7PT-F_2 shows the highest stability, whereas 5PT-CFC-13 has the lowest stability.

From the statistics shown above, it is apparent that as a system's hardness (η) rises, its softness (S) and electrophilicity (ω) decrease, but the stability of a complex structure increases [62]. The high global hardness implies that it is resistant to deformation when subjected to an electric field. Consequently, facilitating the global hardness of material improves its stability while simultaneously reducing the material's reactivity [63, 64]. The value of hardness (η) for 5PT and 7PT is 1.435 and 1.272 eV respectively, and 5PT-CFC-13 and 7PT-CFC-13 show the highest stability.

To get a stronger insight into the electron transfer between the investigated gas molecules and moieties, the parameter ΔN, which indicates the number of fractions of electron transfer between the molecules, was evaluated utilizing Eq. (8). Our estimate, which was conducted using Eq. (11), implies that the values of ΔN are positive, while the values of $\Delta E_{SE(AB)}$ are negative, ranging between − 0.106 and − 1.302 eV (as listed in Table 3 below) for the interaction of examined gas molecules with our explored two moieties. This finding indicates that electrons were transported from moieties to the adsorbate gas molecule, thus establishing the potential of interactions between the investigated adsorbates and adsorbents. The Mulliken electronegativity (χ) analysis is applied to a complex system, to identify the direction in which electrons progress. The term "electronegativity" refers to negative valued chemical potential; $\chi = -\mu$. In this case, electrons act as transmitter medium in a chemical system, which helps to transport electrons from the lower to the higher electronegative area [65]. Table 2 shows that the electronegativity for O_2 (5.843 eV) along with CFCs and F_2 is greater than 5PT (3.467 eV) and 7PT (3.502 eV) except for the complexes of F_2 (5PT-F_2 and 7PT-F_2), which also uncovers the electron transfer from moieties to gas molecules, as anticipated.

Table 3 Fractional charge transfer (ΔN) in Hartree unit, the swap in energy for acceptor, swap in energy for the donor, and the total energy shift for investigated complexes are denoted by $\Delta E_{A(B)}$, $\Delta E_{B(A)}$, and $\Delta E_{SE(AB)}$ in eV respectively

Systems	ΔN	$\Delta E_{A(B)}$	$\Delta E_{B(A)}$	$\Delta E_{SE(AB)}$
5PT-CFC-11	0.366	2.173	1.365	− 0.334
5PT-CFC-12	0.301	1.709	1.108	− 0.243
5PT-CFC-13	0.187	0.952	0.673	− 0.110
5PT-F_2	0.714	5.962	2.841	− 1.285
5PT-O_2	0.990	6.257	4.135	− 1.177
7PT-CFC-11	0.372	2.213	1.391	− 0.332
7PT-CFC-12	0.303	1.722	1.119	− 0.240
7PT-CFC-13	0.187	0.952	0.677	− 0.106
7PT-F_2	0.731	6.127	2.899	− 1.302
7PT-O_2	1.047	6.646	4.364	− 1.225

Table 4 Maximum wavelength of absorption (λ_{max}) in nm, maximum wavelength (λ_{max}) in eV in terms of energy, and oscillation strength (f) for the bare and complex moieties

System	λ_{max} (nm)	λ_{max} (eV)	λ_{max} (eV) shifting	Result	f
5PT	469.563	2.640	-	-	1.591
5PT-CFC-11	471.689	2.629	0.011	Red shift	1.524
5PT-CFC-12	470.829	2.633	0.007	Red shift	1.545
5PT-CFC-13	470.650	2.634	0.006	Red shift	1.563
5PT-F_2	504.079	2.460	0.18	Red shift	0.001
5PT-O_2	458.790	2.702	0.062	Blue shift	1.500
7PT	542.715	2.285	-	-	2.331
7PT-CFC-11	544.216	2.278	0.007	Red shift	2.273
7PT-CFC-12	543.143	2.283	0.002	Red shift	2.301
7PT-CFC-13	530.002	2.340	0.055	Blue shift	2.283
7PT-F_2	542.787	2.284	0.001	Red shift	2.319
7PT-O_2	540.327	2.294	0.009	Blue shift	1.813

Furthermore, separate energy changes in the examined molecules $\Delta E_{A(B)}$, specific energy changes in the studied moieties $\Delta E_{B(A)}$, and the overall change in stabilization energy $\Delta E_{SE(AB)}$ are also explored to get a clear insight into the complexes' stability. As shown in Table 3, the values of $E_{B(A)}$ are positive for all the gas molecules examined that include the two moieties (5PT and 7PT), confirming the spontaneous movement of electrons from moieties to gas molecules. This is often referred to as the "normal electron demand" or NED response [65].

Sensitivity (conductivity) of nPT complexes

Due to the fact that E_g reduction happens in all studied complexes except 5PT-CFC-11, 5PT-CFC-12, and 5PT-CFC-13 (see Table 1), it has a detrimental impact on the distribution of conduction electrons and an electrical signal may generate due to this manner, which is required for the polythiophene moieties to sense or detect gas molecules. The 5PT and 7PT moieties exhibit the following sensitivity to the chosen gas molecules as follows: σ (7PT-F_2) > σ (5PT-F_2) > σ (7PT-O_2) > σ (5PT-O_2) > σ (7PT-CFC-12) > σ (7PT-CFC-11) > σ (7PT-CFC-13). Thus, it can be claimed that 7PT is more sensitive toward selected gas molecules than 5PT.

UV–vis spectra analysis

A study of the ultraviolet–visible spectra of all investigated nanostructures in this existing research was conducted in order to gain a better insight into the interaction among selected gas molecules with the moieties. The

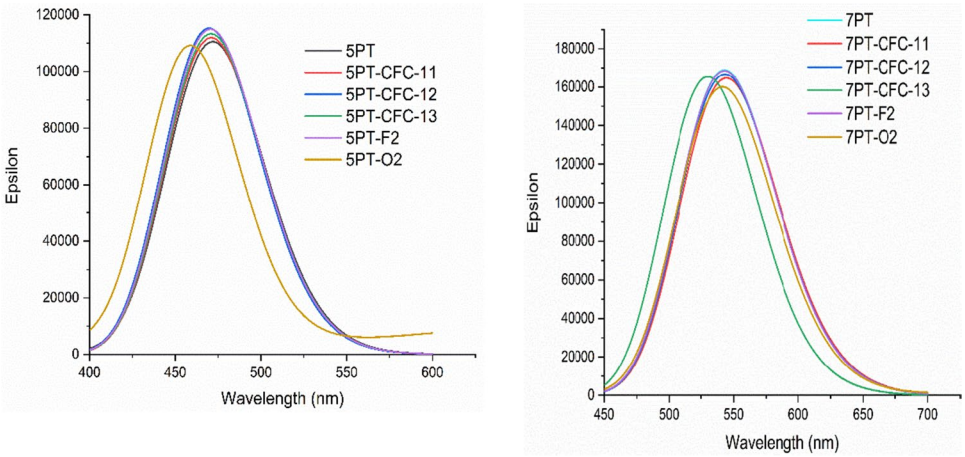

Fig. 7 TD-DFT calculated UV–vis spectra of isolated and complexes of 5PT and 7PT nanostructures

calculations were performed using and choosing the TD-SCF B3LYP/6-31G (d) level of theory with employing 30 number of states. The maximum wavelength of absorption (λ_{max} in nm), the energy-linked with maximum wavelength (λ_{max} in eV), and the strength of oscillation (*f*) for bare and complex moieties are listed in Table 4, and the spectra are displayed in Fig. 7. "The evaluated λ_{max} value of 371 nm for TTP (3.34 eV) simulated by Ali Shokuhi Rad in 2015 had been showing 0.52 eV higher value than the experimental λ_{max} value of nPT is about 440 nm (2.82 eV)" [63]. In our investigation, we get the value of λ_{max} about 469.563 nm (2.640 eV) and 542.715 nm (2.285 eV) for 5PT and 7PT respectively, which are decreased by 0.18 eV and 0.54 eV from experimental value of 440 nm (2.82 eV). This variation is preferable since a vast number of units may be utilized for experimental work of nPT length, while our computation uses just five and seven units. From this observation, it can be confirmed that higher units of polythiophene mean lower λ_{max} eV values (higher λ_{max} nm values). On the other hand, all the values of oscillation strength (*f*) decrease after the adsorption of gas molecules on both the 5PT and 7PT moieties.

As Table 4 shows that following the complexation, the values of λ_{max}, which are attributable to the $\pi \rightarrow \pi*$ transition, are red-shifted for all CFCs and F_2 (except 7PT-CFC-13), and blue-shifted for O_2 for both adsorbent moieties, demonstrating the sensing capacity. After the adsorption of gas molecules on 5PT, a constant wavelength is represented by the spectral peaks for all CFCs, and an observable red shift and blue shift have occurred for 5PT-F_2 and 5PT-O_2, respectively. Besides, for 7PT, the 7PT-CFC-13 and 7PT-O_2 show somewhat changing peaks of spectra confirming slightly blue and red shift, and other peaks remain almost the same. As the maximum wavelength rises, the sensitivity of the adsorbent material increases as well, indicating that new energy states are generated during adsorption [66].

Conclusion

The adsorption of CFCs (CFC-11, CFC-12, CFC-13), F_2, and O_2 on the moieties of nPT (5PT and 7PT as a gas sensor) were examined using DFT calculations. Following geometry optimization of structures, the order of the interaction energies are CFC-11 < F_2 < CFC-12 < CFC-13 < O_2 for both the studied moieties of polythiophene. The electrical structure of HOMO and LUMO indicates that substantial orbital hybridization occurs between CFCs, F_2, and O_2, as well as nPT. A significant shift in the bandgap as a result of the adsorption of the investigated adsorbates was demonstrated by DOS graphs. UV–vis spectra analysis of all the complexes and isolated moieties has been scrutinized. From the fluctuating values of λ_{max}, both red and blue-shifted depending on the complex types. In light of our results, polythiophene might be a suitable gas sensor for detecting the species listed above.

Supplementary Information The online version contains supplementary material available at https://doi.org/10.1007/s00894-022-05048-4.

Acknowledgements We highly acknowledge the software support from the Department of Physics, Computational Condensed Matter Physics Laboratory, Jahangirnagar University, Dhaka, Bangladesh. We thank the Jashore University of Science and Technology (JUST) for letting us run the optimization jobs at the Faculty of Science, Department of Physics.

Author contribution Md. Mehade Hasan and Shahida Aktar Bithe wrote the first draft of the paper. Besides, the first and corresponding author Md. Mehade Hasan has done the formal analysis, data generation, and investigation of the results and discussion part. All authors revised and approved the final version of the manuscript.

Data Availability All data generated or analyzed and related materials (with supplementary materials) are included in this manuscript.

Code availability The calculations have been carried out using Gaussian 09 and GaussView version 6.0 provided by Gaussian, Inc.

Declarations

Conflict of interest The authors declare no competing interests.

References

1. Dubbe A (2003) Fundamentals of solid state ionic micro gas sensors. Sensors Actuators B Chem 88:138–148
2. Zakrzewska K (2001) Mixed oxides as gas sensors. Thin Solid Films 391:229–238
3. Timmer B, Olthuis W, Van Den Berg A (2005) Ammonia sensors and their applications—a review. Sensors Actuators B Chem 107:666–677
4. Nicolas-Debarnot D, Poncin-Epaillard F (2003) Polyaniline as a new sensitive layer for gas sensors. Anal Chim Acta 475:1–15
5. Roncali J (1992) Conjugated poly (thiophenes): synthesis, functionalization, and applications. Chem Rev 92:711–738
6. Ameer Q, Adeloju SB (2005) Polypyrrole-based electronic noses for environmental and industrial analysis. Sensors Actuators B Chem 106:541–552
7. Rad AS, Nasimi N, Jafari M et al (2015) Ab-initio study of interaction of some atmospheric gases (SO_2, NH_3, H_2O, CO, CH_4 and CO_2) with polypyrrole (3PPy) gas sensor: DFT calculations. Sensors Actuators B Chem 220:641–651
8. Ates M, Sarac TK, AS, (2012) Conducting polymers and their applications. Curr Phys Chem 2:224–240
9. Halls JJM, Walsh CA, Greenham NC et al (1995) Efficient photodiodes from interpenetrating polymer networks. Nature 376:498–500
10. Kraft A, Grimsdale AC, Holmes AB (1998) Electroluminescent conjugated polymers—seeing polymers in a new light. Angew Chemie Int Ed 37:402–428
11. Hepburn AR, Marshall JM, Maud JM (1991) Novel electrochromic films via anodic oxidation of carbazolyl substituted polysiloxanes. Synth Met 43:2935–2938
12. Dubois JC, Sagnes O, Henry F (1989) Polyheterocyclic conducting polymers and composites derivates. Synth Met 28:871–878
13. Roncali J, Garreau R, Delabouglise D, et al (1989) Modification of the structure and electrochemical properties of poly (thiophene) by ether groups. J Chem Soc Chem Commun 679–681
14. Bradley DDC (1991) Molecular electronics. Aspects of the physics. Chem Br 27:
15. Gas Sensors Fluorine - Gas-Sensing.com. (n.d.). Retrieved September 3, 2021 from (2000) Ultracapacitors: why, how, and where is the technology. In: Journal of Power Sources. pp 37–50.https://www.gassensing.com/information/fluorin
16. Ullah H, Ayub K, Ullah Z et al (2013) Theoretical insight of polypyrrole ammonia gas sensor. Synth Met 172:14–20
17. Skotheim TA, Reynolds JR (2007) Handbook of conducting polymers: conjugated polymers processing and applications
18. Virji S, Huang J, Kaner RB, Weiller BH (2004) Polyaniline nanofiber gas sensors: examination of response mechanisms. Nano Lett 4:491–496
19. Friend RH, Gymer RW, Holmes AB et al (1999) Electroluminescence in conjugated polymers. Nature 397:121–128
20. Ma X, Li G, Xu H et al (2006) Preparation of polythiophene composite film by in situ polymerization at room temperature and its gas response studies. Thin Solid Films 515:2700–2704
21. Molina MJ, Rowland FS (1974) Stratospheric sink for chlorofluoromethanes-chlorine atom catalyzed destruction of ozone. In: International Conference on the Environmental Impact of Aerospace Operations in the High Atmosphere, 2 nd, San Diego, Calif. pp 99–104
22. Kim K-H, Shon Z-H, Nguyen HT, Jeon E-C (2011) A review of major chlorofluorocarbons and their halocarbon alternatives in the air. Atmos Environ 45:1369–1382
23. UNEP (2006) The Montreal protocol on substances that deplete the ozone layer
24. McCulloch A, Ashford P, Midgley PM (2001) Historic emissions of fluorotrichloromethane (CFC-11) based on a market survey. Atmos Environ 35:4387–4397
25. Metz, Bert M, Kuijpers L, Solomon S, et al (2005) Safeguarding the ozone layer and the global climate system: issues related to hydrofluorocarbons and perfluorocarbons
26. (2002) Toxicological profile for carbon tetrachloride. In: ATSDR's Toxicological Profiles
27. Midgley T Jr (1937) From the periodic table to production. Ind Eng Chem 29:241–244
28. McCulloch A, Midgley PM, Ashford P (2003) Releases of refrigerant gases (CFC-12, HCFC-22 and HFC-134a) to the atmosphere. Atmos Environ 37:889–902
29. Siegemund G, Schwertfeger W, Feiring A, et al (2000) Fluorine compounds, organic. Ullmann's Encycl Ind Chem
30. Oğuz I-C, Mineva T, Guesmi H (2018) The effect of Pd ensemble structure on the O2 dissociation and CO oxidation mechanisms on Au—Pd (100) surface alloys. J Chem Phys 148:24701
31. Murray JS, Seybold PG, Politzer P (2021) The many faces of fluorine: some noncovalent interactions of fluorine compounds. J Chem Thermodyn 156:106382. https://doi.org/10.1016/j.jct.2020.106382
32. Gas sensors fluorine - gas-sensing.com. (n.d.) Retrieved September 3, 2021, https://www.gassensing.com/information/fluorine.
33. Cabrera N, Mott NF (1949) Theory of the oxidation of metals. Reports Prog Phys 12:163–184
34. Sun S, Xu P, Ren Y et al (2018) First-principles study of dissociation processes of O2 molecular on the Al (111) surface. Curr Appl Phys 18:1528–1533
35. Rakib Hossain M, Mehade Hasan M, Ud Daula Shamim S et al (2021) First-principles study of the adsorption of chlormethine anticancer drug on C24, B12N12 and B12C6N6 nanocages. Comput Theor Chem 1197:113156. https://doi.org/10.1016/j.comptc.2021.113156
36. Shokuhi Rad A, Zardoost MR, Abedini E (2015) First-principles study of terpyrrole as a potential hydrogen cyanide sensor: DFT calculations. J Mol Model 21:273. https://doi.org/10.1007/s00894-015-2814-y
37. Rad AS, Zardoost MR, Abedini E (2015) First-principles study of terpyrrole as a potential hydrogen cyanide sensor: DFT calculations. J Mol Model 21:1–7
38. Tenderholt AL, Langner KM, O'Boyle NM (2008) A library for package-independent computational chemistry algorithms. J Comp Chem 839–845
39. MM Hasan AC Das MR Hossain et al 2021 The computational quantum mechanical investigation of the functionalized boron nitride nanocage as the smart carriers for favipiravir drug delivery: a DFT and QTAIM analysis J BiomolStruct Dyn 1 17. https://doi.org/10.1080/07391102.2021.1982776
40. MM Hasan MH Kabir MA Badsha MR Hossain 2021 A first-principles DFT study on the adsorption behaviour of CO, CO2, and O3 on pristine B24N24 and silicon-decorated B24N24 nanosheet Phosphorus Sulfur Silicon Relat Elem 1–8. https://doi.org/10.1080/10426507.2021.1988599
41. Rad AS (2015) Al-doped graphene as modified nanostructure sensor for some ether molecules: Ab-initio study. Synth Met 209:419–425
42. Kamel M, Raissi H, Morsali A, Shahabi M (2018) Assessment of the adsorption mechanism of Flutamide anticancer drug on the functionalized single-walled carbon nanotube surface as a drug

delivery vehicle: an alternative theoretical approach based on DFT and MD. Appl Surf Sci 434:492–503
43. Saha S, Roy RK, Pal S (2010) CDASE—a reliable scheme to explain the reactivity sequence between Diels-Alder pairs. Phys Chem Chem Phys 12:9328–9338
44. Sarmah A, Roy RK (2013) Understanding the interaction of nucleobases with chiral semiconducting single-walled carbon nanotubes: an alternative theoretical approach based on density functional reactivity theory. J Phys Chem C 117:21539–21550
45. MR Hossain MM HasanAshrafi N-E- et al 2021 Adsorption behaviour of metronidazole drug molecule on the surface of hydrogenated graphene, boron nitride and boron carbide nanosheets in gaseous and aqueous medium: a comparative DFT and QTAIM insight Phys E Low-dimensional Syst Nanostructures 126 114483. https://doi.org/10.1016/j.physe.2020.114483
46. Li J, Lu Y, Ye Q et al (2003) Carbon nanotube sensors for gas and organic vapor detection. Nano Lett 3:929–933
47. Ahmadi Peyghan A, Hadipour NL, Bagheri Z (2013) Effects of Al doping and double-antisite defect on the adsorption of HCN on a BC2N nanotube: density functional theory studies. J Phys Chem C 117:2427–2432
48. Ahmadi A, Hadipour NL, Kamfiroozi M, Bagheri Z (2012) Theoretical study of aluminum nitride nanotubes for chemical sensing of formaldehyde. Sensors Actuators B Chem 161:1025–1029. https://doi.org/10.1016/j.snb.2011.12.001
49. Rad AS, Shabestari SS, Jafari SA et al (2016) N-doped graphene as a nanostructure adsorbent for carbon monoxide: DFT calculations. Mol Phys 114:1756–1762
50. Maria JP, Nagarajan V, Chandiramouli R (2020) Boron trifluoride interaction studies on graphdiyne nanotubes–a first-principles insight. Chem Phys Lett 738:136841
51. Diaz AF, Crowley J, Bargon J et al (1981) Electrooxidation of aromatic oligomers and conducting polymers. J Electroanal Chem Interfacial Electrochem 121:355–361
52. Rad AS, Abedini E (2016) Chemisorption of NO on Pt-decorated graphene as modified nanostructure media: a first principles study. Appl Surf Sci 360:1041–1046
53. Bulat FA, Murray JS, Politzer P (2021) Identifying the most energetic electrons in a molecule: the highest occupied molecular orbital and the average local ionization energy. Comput Theor Chem 1199:113192. https://doi.org/10.1016/j.comptc.2021.113192
54. Murray JS, Politzer P (2017) Molecular electrostatic potentials and noncovalent interactions. Wiley Interdiscip Rev Comput Mol Sci 7:e1326
55. Murray JS, Politzer P (2009) Molecular surfaces, van der Waals radii and electrostatic potentials in relation to noncovalent interactions. Croat Chem Acta 82:267–275
56. Shamim SUD, Miah MH, Hossain MR et al (2022) Theoretical investigation of emodin conjugated doped B12N12 nanocage by means of DFT, QTAIM and PCM analysis. Phys E Low-dimensional Syst Nanostructures 136:115027. https://doi.org/10.1016/j.physe.2021.115027
57. Politzer P, Murray JS (2021) Are HOMO–LUMO gaps reliable indicators of explosive impact sensitivity? J Mol Model 27:327. https://doi.org/10.1007/s00894-021-04956-1
58. Rad AS (2016) Adsorption of C2H2 and C_2H_4 on Pt-decorated graphene nanostructure: ab-initio study. Synth Met 211:115–120
59. Rad AS (2015) Application of polythiophene to methanol vapor detection: an ab initio study. J Mol Model 21:1–6
60. Job G, Herrmann F (2006) Chemical potential—a quantity in search of recognition. Eur J Phys 27:353
61. Cook G, Dickerson RH (1995) Understanding the chemical potential. Am J Phys 63:737–742
62. Rad AS (2016) Al-doped graphene as a new nanostructure adsorbent for some halomethane compounds: DFT calculations. Surf Sci 645:6–12
63. Rad AS (2016) Terthiophene as a model sensor for some atmospheric gases: theoretical study. Mol Phys 114:584–591. https://doi.org/10.1080/00268976.2015.1102348
64. Rad AS, Valipour P (2015) Interaction of methanol with some aniline and pyrrole derivatives: DFT calculations. Synth Met 209:502–511
65. Kamel M, Raissi H, Morsali A (2017) Theoretical study of solvent and co-solvent effects on the interaction of Flutamide anticancer drug with carbon nanotube as a drug delivery
66. H Sajid S Khan K Ayub T Mahmood 2020 High selectivity of cyclic tetrapyrrole over tetrafuran and tetrathiophene toward toxic chemicals; a first-principles study MicroporousMesoporous Mater 299. https://doi.org/10.1016/j.micromeso.2020.110126